Centrality dependence in J/Ψ photoproduction in pp, pA and AA collisions

M. B. Gay Ducati and P. H. Fetter da Luz
GFPAE - Department of Physics, UFRGS, Porto Alegre - BR

The photoproduction of J/Ψ is investigated in the coherent collisions at LHC energy ($\sqrt{s}$ = 5.02 TeV), for distinct transverse momentum and centrality classes: ultra-peripheral collisions (UPC) and peripheral collisions across different event geometries. An application of the convolution between the photon flux and the photonuclear cross section is explored for UPCs. In the peripheral regime, different centrality classes were tested (30%-50%, 50%-70%, and 70%-90%) considering an effective photon flux constraining the geometrical region of the nuclei-target. Consistently, an effective photonuclear cross section was applied. The low-x formulation for the distinct geometries, allows the comparison of three dipole models, suited for saturation. Results for both rapidity and transverse momentum distributions are presented and compared to ALICE and LHCb data showing good agreement.

DOI: https://doi.org/10.17161/stfvrt42

Keywords: Photoproduction, ultra-peripheral collisions, dipole models, photonuclear cross section

1 Introduction

In QCD, the production cross sections of hadronic interactions can be factorized, i.e., it can be described as a convolution between the parton distribution functions $f_i(x, Q^2)$, the PDFs, with the cross section of the involved partonic subprocess $\hat{\sigma}$. The PDFs describe the probability of finding a parton i with a fraction of momentum x of the longitudinal hadron, when probed in a determined energy scale Q^2. These functions are universal, that is, they are the same in any kind of process. Therefore, if we find the PDF for a deep inelastic process, for example, it will be the same for a hadroproduction process. The results using HERAPDF [2] for the proton PDF show that, for high values of the Björken-x ($x \approx 1$) the valence quarks dominate. We are in the perturbative regime of QCD, where the evolution can be described by linear equations such as DGLAP [3,4,5] and BFKL [6]. The divergences occur at very high energy, where we have small-x ($x < 10^{-2}$). Here the sea quarks and the gluons are predominant. There is a rapid growth in the gluon density, because they can unfold into a pair of gluons ($g \to gg$), multiplying their number. This happens until the saturation limit, in which effects like gluon recombination counterbalance their growth, leading to a dynamical scale called the saturation scale $Q_s(x)$. At this point, the break of the linear regime occurs, and the evolution equations begin to be described by non-linear equations, such as AGL [7], JIMWLK [8,9,10] and BK [11,12]. Therefore, this non-linear regime defines a new QCD frontier, so that studying photon-induced processes, such as ultra-peripheral collisions (UPCs) and the dipole formalism provide a powerful framework to probe the saturation effects and the dynamics at small-x physics.

The ultra-peripheral collisions of heavy ions at high energy present an opportunity to study processes where the Color Dipole Formalism can be applied. In these collisions, the distance between both nuclei, called the impact parameter (b), is larger than the sum of their radii. In this condition, the UPC process can be described as a purely electromagnetic process because there is no direct hadronic collision involved. Thus, in the dipole formalism, the virtual photon from one nucleus interacts with the target; it splits into a quark-antiquark pair ($q\bar{q}$). This pair will interact with the target by gluon exchange. Moreover, these quarks could emit soft gluons that also could emit softer gluons ($g \to gg$). In this process, the gluon distribution will grow considerably, until the recombination effect ($gg \to g$) compensates this multiplicity, reaching the saturation, predicted by the formalism.

As mentioned, the UPC of heavy ions can give access to the gluon distribution, contributing to understanding QCD in this saturation limit. We can probe this limit by measuring the vector mesons that could be produced in this collision. By the dipole formalism, the virtual quark will split into a $q\bar{q}$ pair that interacts with the target due to the gluon exchange. After this interaction, the $q\bar{q}$ pair can hadronize into a vector meson, like the J/Ψ resonance, the Υ resonance, or their excited states. Figure 1 shows the two possibilities for this photoproduction, the exclusive photoproduction, where the final

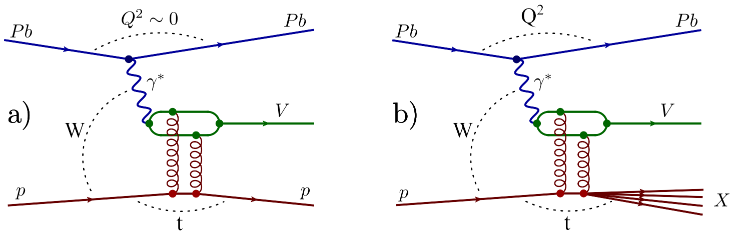

Figure 1 – a) Exclusive photoproduction: The final state is known, there are no additional particles. b) Inclusive photoproduction: high multiplicity of particles in the final state.

state is well defined with no additional particles (Figure 1 panel a). This process is characterized by a large rapidity gap and the event can be totally reconstructed. The other possibility is the inclusive photoproduction, where the final products are composed of a higher multiplicity of particles and there are other particles produced due to fragmentation and no rapidity gap (Figure 1 panel b).

The process presented here is the exclusive photoproduction of vector mesons in UPC ($b > R_A + R_A$) and also, an extension to the peripheral case ($b < R_A + R_A$). To calculate the cross section of this process, the Weizsäcker-Williams method will be utilized, where the cross section can be described by the convolution between the photon flux that interacts with the target and the cross section of this interaction, the photonuclear cross section. Additionally, for the peripheral approach, three scenarios will be investigated to describe the cross section of the photoproduction. In the first scenario (S1) there is no modification on the photon flux and the photonuclear cross section; the same as in the UPC case is used. On the other hand, in scenario 2 (S2), a modification in the photon flux is made to consider that only the spectator interacts coherently with the photon. Complementarily, in scenario 3 (S3), in addition to the effective photon flux, the photonuclear cross section is also modified with the same hypothesis.

This work presents the calculations using the models described above, applied to both ultra-peripheral and peripheral collisions. In the UPC case, the model will be compared with ALICE data for the J/Ψ photoproduction and the $\Psi(2s)$. Also, results for the Υ and $\Upsilon(2s)$ photoproduction will be provided. In the peripheral case, using the model presented above, the results corresponding to different centralities for the J/Ψ photoproduction are shown. Together, these analyses aim to contribute to a deeper insight into the photon-induced process which can probe the small-x structure of nuclear matter.

2 Theoretical framework

As mentioned before, applying the Weizsäcker-Williams method, the hadron-hadron interaction is described as a photon-hadron interaction. Therefore, the main ingredients to determine the cross section of the vector meson photoproduction, in both pp and A-A collisions, are the photon flux ($N_\gamma^{h_A}$) and the photonuclear cross section ($\sigma_V^{\gamma h_A}$). For any hadron-hadron collisions ($h_A + h_B$), it can be written as

$$\frac{d\sigma}{dy}(h_A h_B \to h_A \otimes V \otimes h_B) = \omega(y) N_\gamma^{h_A}(\omega(y)) \sigma_V^{\gamma h_B}(\omega(y)) + (y \to -y) \tag{1}$$

with ω being the photon energy and y the rapidity. The second term in this equation is due to the symmetry of the collision, where there is an ambiguity in the photon emitter, the nucleus either acts as the source of photons or acts as the target.

The photon flux can be determined using principles from electrodynamics, where it can be described in terms of the energy distribution per unit of area and frequency.

$$\frac{d^3N}{d\omega d^2b} = \frac{1}{\omega}\frac{dI}{d\omega}$$

Integrating in terms of the impact parameter over a lower limit $b_{min} = R_A$ and after some algebraic manipulation, where the modified Bessel functions of the second kind (K_0 and K_1) are used [13], we get

$$\frac{dI(\omega)}{d\omega} = \frac{2q^2}{\pi}\left[\chi_{min} K_0(\chi_{min}) K_1(\chi_{min}) - \frac{1}{2}\chi_{min}^2 [K_1^2(\chi_{min}) - K_0^2(\chi_{min})]\right] \tag{2}$$

with $\chi_{min} = \omega R_A/\gamma$.

To evaluate the photonuclear interaction, the dipole formalism predicts a factorization in the cross section. For the $\gamma - p$ interaction, the amplitude of the process is given by [14]

$$\mathrm{Im}A_{proton}(x, t = 0) = \int\int \frac{d^2 r dz}{4\pi} \left(\Psi_V^* \Psi_\gamma\right)_T \sigma_{dip}^{proton}(x, r) \tag{3}$$

where the $(\Psi_V^* \Psi_\gamma)_T$ is the overlap photon-meson wave function, which represents the probability of a $q\bar{q}$ pair hadronizing into a vector meson after the interaction with the target. The wave functions are different for photons with polarization transversal or longitudinal; however, for the UPCs, the photons are almost real, so the transversal term is dominant. Additionally, these functions can be modeled phenomenologically by the Boosted Gaussian model [15].

The other term in the amplitude function is the proton-dipole cross section ($\sigma_{dip}^{proton}(x, r)$), which will describe the probability amplitude of interaction between the color dipole ($q\bar{q}$) with the target. There are several parameterizations that can be applied, in this work, it will be tested the GBW [16], the CGC [17] and the bCGC [18].

For the $\gamma - A$ interaction, the amplitude is similar to the one in the γ-p interaction, with a change, replacing the ($\sigma_{dip}^{proton}(x, r)$) for the ($\sigma_{dip}^{nuc}(x, r)$), where the nuclear-dipole cross section can be written in terms of the proton-dipole cross section [19].

$$\sigma_{dip}^{nuc}(x, r) = 2 \int d^2 b' \left[1 - \exp\left(-\frac{1}{2} T_A(b') \sigma_{dip}^{proton}(x, r)\right)\right] \tag{4}$$

with b' the photon-nuclei impact parameter. The $T_A(b')$ term is the nuclear profile function, which can be described in relation to the nuclear density as $T_A(\vec{r}) = \int dz \rho_A(\sqrt{|\vec{r}|^2 + z^2})$. For heavy nuclei, the density ρ_A is typically parameterized using a Woods-Saxon distribution.

For the peripheral case, the impact parameter b is smaller than the sum of the radii of the colliding nuclei. Therefore, a new quantity can be defined to describe the geometry of the collision, i.e., if the collision is more central or peripheral. This quantity is the centrality, which, for A-A collision, can be represented in the purely geometric way as $c = \frac{b^2}{4R_A^2}$.

Thus, for the centrality class in the range 30% - 50%, the collision is close to a central collision, and for 70% - 90% it is almost an ultra-peripheral collision. The present contribution explores the peripheral collisions for three centrality classes, 30% - 50%, 50% - 70%, and 70% - 90% in three different scenarios to calculate the cross section. The first scenario (S1) only considers a dependence on the impact parameter for the photon flux. There is no modification on the photonuclear cross section.

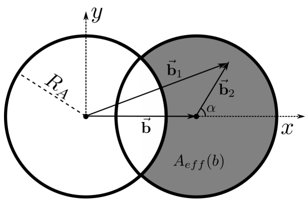

Figure 2 – Scheme of interaction for both scenario 2 and 3 of the peripheral collision, where one considers that only the spectators photons, those that reach the geometrical region, interact coherently with the target.

For scenario 2 and 3, a change in the photon flux and in the photonuclear cross section is built considering that only spectators interact coherently with the photon, Figure 2. It is based on the hypothesis that only photons that reach the geometrical region of the target will be considered in the calculations and any photon that reaches the overlap region will be neglected. In scenario 2 (S2) an effective photon flux is developed under this hypothesis, such that it can be expressed as [20]

$$N^{eff}(\omega, b) = \frac{1}{A_{eff}(b)} \int N^{usual}(\omega, b_1) \theta(b_1 - R_A) \theta(R_A - b_2) d^2 b_2 \tag{5}$$

with the effective interaction area given by $A_{eff}(b) = R_A^2 \left[\pi - 3\cos^{-1}\left(\frac{b}{2R_A}\right)\right] + \frac{b}{2}\sqrt{4R_A^2 - b^2}$. In addition to the effective photon flux, scenario 3 (S3) will also modify the photonuclear cross section employing the same geometrical constraints, which is done by $\theta(b_1 - R_A)$ into Eq. (4), thus

$$\sigma_{dip}^{nuc}(x,r) = 2\int d^2b_2\theta(b_1 - R_A)\left[1 - \exp\left(-\frac{1}{2}T_A(b_2)\sigma_{dip}^{proton}(x,r)\right)\right] \tag{6}$$

where $b_1^2 = b^2 + b_2^2 + 2bb_2\cos(\alpha)$.

Considering these three scenarios for the peripheral case, and the UPC process, the next section will present the results for the rapidity distribution of the cross section for lead-lead collisions (UPC and peripheral) and pp, pPb collisions (for UPC).

3 Main Results

The Figure 3 and 4 left present the rapidity distribution for ultra-peripheral collisions of pp compared with the LHCb data [21] at 7 TeV. These results are for the photoproduction of the J/Ψ, the $\Psi(2s)$, and the Υ vector meson. In both photoproductions, the GBW dipole model overestimates the data, and for the $\Psi(2s)$ photoproduction, the CGC and bCGC models underestimate it. In contrast, the CGC and bCGC models are consistent with the data of the J/Ψ and Υ [22].

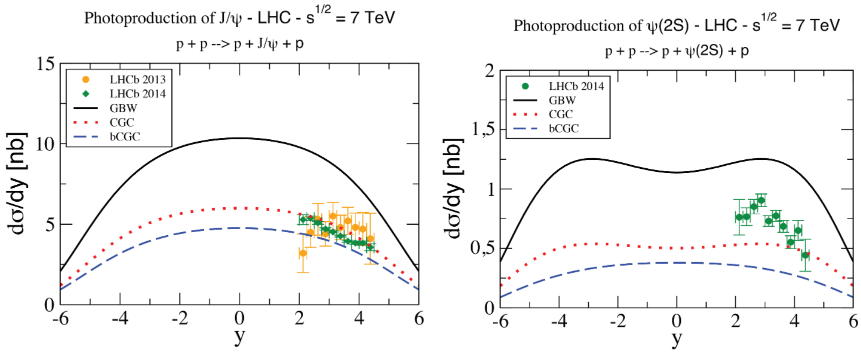

Figure 3 – Coherent J/Ψ (left) and $\Psi(2S)$ (right) photoproduction in pp collisions at 7 TeV calculated for the dipole models GBW, CGC and bCGC and compared with LHCb data [27,28].

For the pPb UPC (right side of Figure 4), the rapidity distribution of the photoproduction of the J/Ψ particle is compared with ALICE data [23]. As before, the CGC and bCGC provide good agreement with the data, and the GBW overestimates the data from ALICE in the whole interval of rapidity.

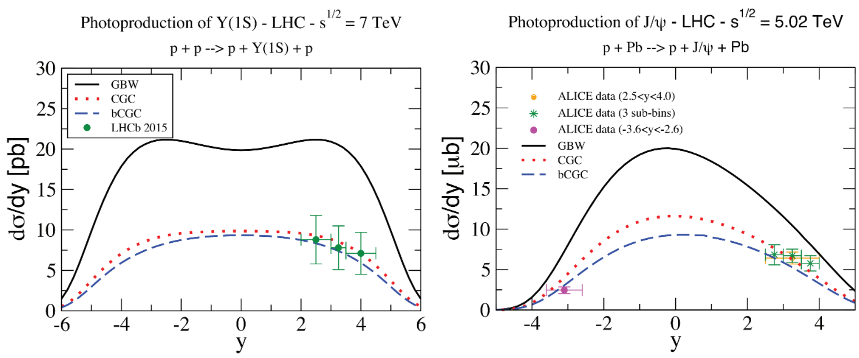

Figure 4 – Left) Coherent Υ photoproduction in pp collisions at 7 TeV. Right) Coherent J/Ψ photoproduction in p-Pb at 5.02 TeV. The cross sections are calculated for the dipole models GBW, CGC and bCGC and compared with LHCb data[22] (left) and ALICE data[23] (right).

The UPC results for the photoproduction of the J/Ψ and $\Psi(2s)$ in Pb-Pb collisions at 5.02 TeV are compared with ALICE data [24] in the Figure (5), where, in the forward region of the rapidity, all models underestimate the data, but, they are able to reproduce the overall trend. For the central rapidity, the models overestimate the results from ALICE, with the bCGC showing the best agreement. In the same figure, it is also shown the results for the Υ and $\Upsilon(2s)$ photoproduction.

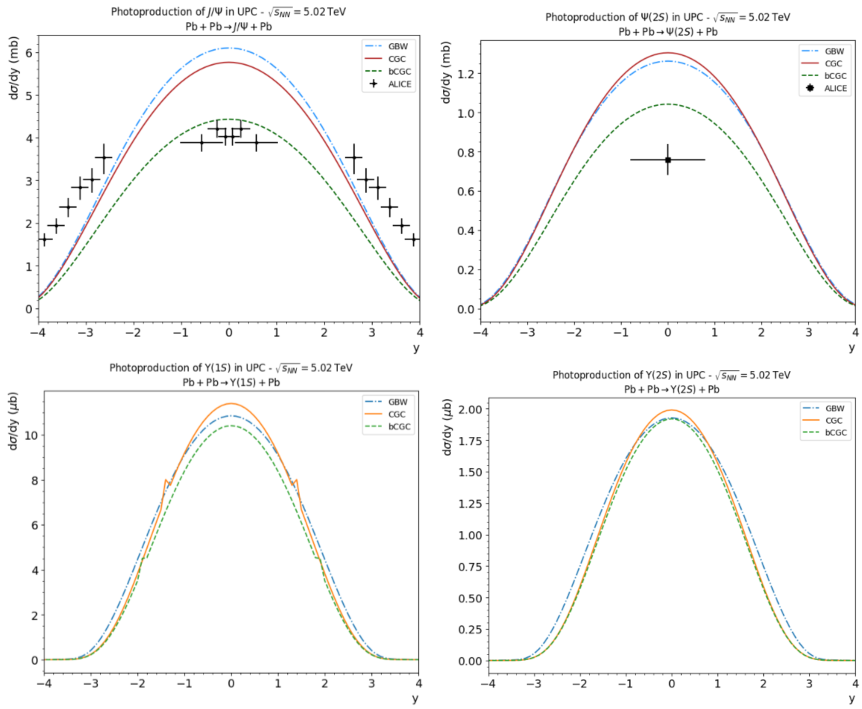

Figure 5 – Top (bottom) Coherent J/Ψ and $\Psi(2S)$ (Υ and $\Upsilon(2S)$) photoproduction in UPC Pb-Pb collisions at 5.02 TeV. The results are calculated using GBW, CGC and bCGC models and compared with ALICE data[24].

The peripheral results are shown in Figure (6) for the photoproduction of the J/Ψ in lead-lead collisions at 5.02 TeV, calculated in the three scenarios. The S2 and S3 reduce the cross section when compared to S1 due to the cut imposed by the hypothesis that only spectators will interact with the target. The bottom right plot of the figure shows the coherent J/Ψ cross section as a function of $< N_{part} >$ measured by ALICE [25,26] at midrapidity for the centrality classes 70-90%, 50-70% and 40-50%. These data are compared with the S2 and S3 for the dipole models GBW and CGC (IIM) showing that all models overestimate the values, with the S3 being the most compatible overall.

4 Conclusion

The present results of UPC for pp and pPb collisions demonstrate that the dipole formalism has good agreement with the experimental data when it is used in both CGC and bCGC models. However, the GBW model overestimates the data in all productions. For the lead-lead collisions, the formalism can represent the shape and the overall trend of the data, but still underestimates it. Regarding the peripheral case, the inclusion of geometric constraints, as proposed in scenarios 2 and 3, reduces the cross section overall. These results compared with ALICE data show that scenario 3 has the most compatible values; nevertheless, all models are still unable to reproduce the data in more central collisions. In light of this, the search for a refined theory that can incorporate and implement the low-x phenomenology is still needed. Moreover, future analysis of new data at different centralities may provide constraints and contribute to extracting more precisely the gluon distribution function.

5 Acknowledgments

We acknowledge the financial support from CNPq, which enabled this research. We also wish to thank Laure Marie Massacrier and Afnan Shatat for useful discussions that contributed to this work.

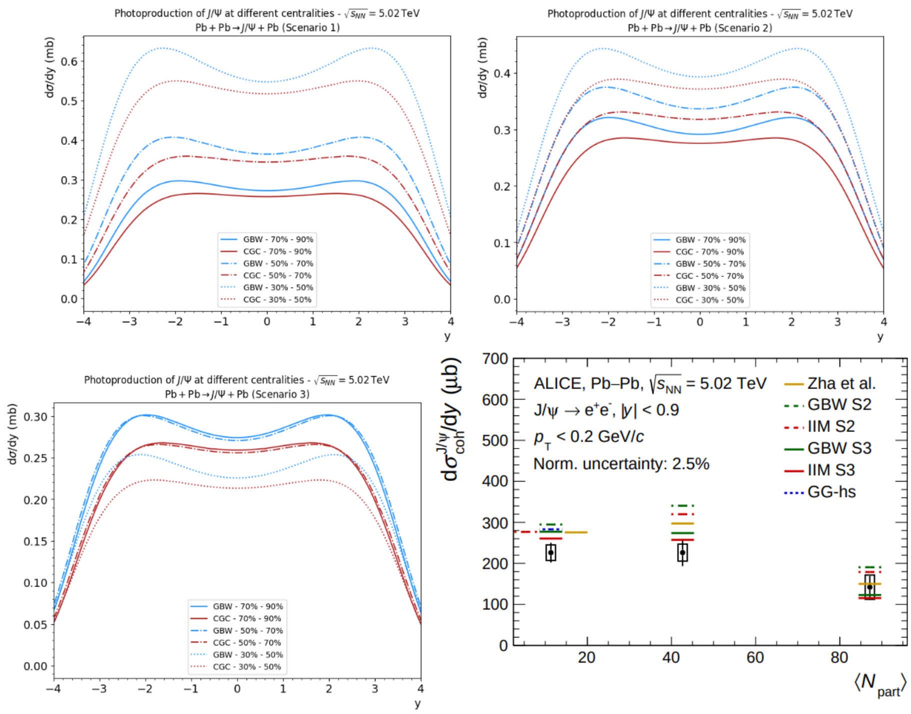

Figure 6 – Top and bottom left) Coherent J/Ψ photoproduction in Pb-Pb collisions at 5.02 TeV for different centralities. The cross sections are calculated for the dipole models GBW, CGC and bCGC with the three scenarios. Bottom right) The coherent J/Ψ production as a function of $< N_{part} >$ measured by ALICE[25,26].

References

1. C. A. Bertulani and G. Baur, Phys. Rept. **163**, 299 (1988) doi:10.1016/0370-1573(88)90142-1
2. H1 and ZEUS Collaborations, arXiv:1506.06042 [hep-ex].
3. V. N. Gribov and L. N. Lipatov, Sov. J. Nucl. Phys. **15**, 438 (1972).
4. G. Altarelli and G. Parisi, Nucl. Phys. B **126**, 298 (1977) doi:10.1016/0550-3213(77)90384-4.
5. Y. L. Dokshitzer, Sov. Phys. JETP **46**, 641 (1977).
6. Y. V. Kovchegov and E. Levin, Oxford University Press, 2013 doi:10.1017/9781009291446.
7. A. L. Ayala, M. B. Gay Ducati and E. M. Levin, Nucl. Phys. B **493**, 305 (1997) doi:10.1016/S0550-3213(97)00002-3.
8. E. Iancu, A. Leonidov and L. McLerran, Nucl. Phys. A **692**, 583 (2001) doi:10.1016/S0375-9474(01)00642-X.
9. E. Ferreiro, E. Iancu, A. Leonidov and L. McLerran, Nucl. Phys. A **703**, 489 (2002) doi:10.1016/S0375-9474(01)01329-X.
10. J. Jalilian-Marian, A. Kovner, A. Leonidov and H. Weigert, Nucl. Phys. B **504**, 415 (1997) doi:10.1016/S0550-3213(97)00440-9.
11. I. Balitsky, Nucl. Phys. B **463**, 99 (1996) doi:10.1016/0550-3213(95)00638-9.
12. Y. V. Kovchegov, Phys. Rev. D **60**, 034008 (1999) doi:10.1103/PhysRevD.60.034008.
13. W. Magnus, F. Oberhettinger and R. P. Soni, Springer-Verlag, New York, 1966.
14. N. Armesto, Eur. Phys. J. C **26**, 35 (2002) doi:10.1007/s10052-002-1021-z.
15. J. R. Forshaw, R. Sandapen and G. Shaw, Phys. Rev. D **69**, 094013 (2004) doi:10.1103/PhysRevD.69.094013.
16. K. Golec-Biernat and M. Wüsthoff, Phys. Rev. D **59**, 014017 (1998) doi:10.1103/PhysRevD.59.014017.
17. E. Iancu, K. Itakura and S. Munier, Phys. Lett. B **590**, 199 (2004) doi:10.1016/j.physletb.2004.02.040.
18. H. Kowalski, L. Motyka and G. Watt, Phys. Rev. D **74**, 074016 (2006) doi:10.1103/PhysRevD.74.074016.
19. V. N. Gribov, Sov. Phys. JETP **29**, 483 (1969).
20. M. B. Gay Ducati and S. Martins, PoS **ICHEP2018**, 602 (2019) doi:10.22323/1.340.0602.
21. R. Aaij *et al.*, J. Phys. G: Nucl. Part. Phys. **40**, 045001 (2013).

22. R. Aaij *et al.*, JHEP **09**, 084 (2015) doi:10.1007/JHEP09(2015)084.
23. B. Abelev *et al.* [ALICE Collaboration], Phys. Rev. Lett. **113**, 232504 (2014) doi:10.1103/PhysRevLett.113.232504.
24. M. B. Gay Ducati, F. Kopp, M. V. T. Machado, and S. Martins, Phys. Rev. D **94**, 094023 (2016) doi:10.1103/PhysRevD.94.094023.
25. S. Acharya *et al.* [ALICE Collaboration], Phys. Lett. B **798**, 134926 (2019) doi:10.1016/j.physletb.2019.134926.
26. S. Acharya *et al.* [ALICE Collaboration], Eur. Phys. J. C **81**, 712 (2021) doi:10.1140/epjc/s10052-021-09672-5.
27. R. Aaij *et al.* [LHCb Collaboration], J. Phys. G **40**, 045001 (2013) doi:10.1088/0954-3899/40/4/045001.
28. R. Aaij *et al.* [LHCb Collaboration], J. Phys. G **41**, 055002 (2014) doi:10.1088/0954-3899/41/5/055002.